

Minimally Invasive Temperature Mapping for Laser Ablation: A Preliminary Study on Ex-vivo Livers

*Original*

Minimally Invasive Temperature Mapping for Laser Ablation: A Preliminary Study on Ex-vivo Livers / Bellone, A., Olivero, M., Coppa, G., Vallan, A., Perrone, G.. - In: IEEE TRANSACTIONS ON INSTRUMENTATION AND MEASUREMENT. - ISSN 0018-9456. - STAMPA. - 74:(2025). [10.1109/TIM.2025.3551467]

*Availability:*

This version is available at: 11583/2999026 since: 2025-06-16T09:02:38Z

*Publisher:*

IEEE

*Published*

DOI:10.1109/TIM.2025.3551467

*Terms of use:*

This article is made available under terms and conditions as specified in the corresponding bibliographic description in the repository

*Publisher copyright*

IEEE postprint/Author's Accepted Manuscript

©2025 IEEE. Personal use of this material is permitted. Permission from IEEE must be obtained for all other uses, in any current or future media, including reprinting/republishing this material for advertising or promotional purposes, creating new collecting works, for resale or lists, or reuse of any copyrighted component of this work in other works.

(Article begins on next page)

# Minimally Invasive Temperature Mapping for Laser Ablation: A Preliminary Study on Ex-vivo Livers

Aurora Bellone, Massimo Olivero, Gianni Coppa,  
Alberto Vallan, *Senior Member, IEEE*, Guido Perrone, *Member, IEEE*

**Abstract**—The optimization of laser ablation surgical procedures – specifically for the treatment of tumors – requires evaluating the temperature distribution across the entire area under treatment (e.g., the tumor volume). However, minimally invasive temperature sensors can only provide information in a limited number of points. Therefore, an effective prediction algorithm is required to reconstruct the temperature map for the entire heat affected tissue from as few temperature measurements as possible. This work presents an approach for predicting the temperature around the laser delivery fiber, based on the thermal Green’s function, where patient-specific tissue thermal parameters are obtained through a fitting procedure using measurement of the temperature evolution at known locations. The proposed method is independent of the specific temperature sensor used; in the experiments reported, temperature was measured both at the prediction points and at validation points using quasi-distributed sensor composed of dense fiber Bragg grating (FBG) arrays, written with a femtosecond laser. A preliminary validation under ideal conditions, represented by ex-vivo cases, has been performed through a series of experiments on bovine liver samples. The obtained results demonstrate that it is possible to predict the temperature distribution across the entire ablated area, with errors well below the commonly accepted uncertainty for treatments of this type.

**Index Terms**—Tumor laser ablation, Thermal parameter of biological tissues, Fiber Bragg grating temperature sensors, Fiber Bragg grating sensor array, Heat Pulse Method.

## I. INTRODUCTION

Minimally invasive high-temperature thermal treatments – the so-called “ablations” – are a set of rather novel therapies for the treatment of solid tumors, which can be used either as adjuvants or as alternatives to more consolidated approaches, such as surgical resection, radiotherapy, or chemotherapy. In particular, these thermal treatments, which require to locally increase the temperature above about 55 °C to ensure the immediate necrosis of malignant cells [1], [2], are mostly attractive for patients who are not eligible for traditional surgery. Different implementations are described in the literature depending on the heat source, namely radio-frequency, microwave, or laser ablations. Sometimes the effects of these thermal treatments are enhanced through the use of nanoparticles that acts as sensitizers or as radiation absorbers [3]. Each

solution has its own strengths, but they all share the advantage of causing less discomfort to the patient and of implying lower overall costs, being less traumatic and requiring fewer days of hospitalization. This paper specifically addresses the case of Laser Ablation (LA) without the use of additional nanoparticles, but many of the conclusions are expected to be straightforwardly applied also to the other heating techniques. LA uses high-power laser beams, up to about 10 W, typically generated by laser diodes emitting in the 905 nm to 980 nm range since these wavelengths represent a good compromise between localization of the heating due to the absorption by the tissue and extension of the treated area [4]. In the case of tumors affecting internal organs, the laser beam is delivered using a large core fiber inserted through the skin with a needle, which is accurately positioned via ultrasound image guiding, magnetic resonance or computed tomography [5]. Since the effects of LA are predominantly thermal, the optimization of the outcomes requires real-time knowledge of the temperature distribution across the entire treated area [2]. In fact, this would allow for fine-tuning the process to ensure that the temperature reaches the target value to induce necrosis in malignant cells and at the same time spare the surrounding healthy tissues [1], [6]. While the surgeon’s expertise can make real-time temperature monitoring less critical, a more widely accepted approach is to complement subjective expertise with objective temperature measurements, rather than relying solely on image interpretation and experience. The significance of accurate temperature determination is well-recognized, even in the precursors to LA, such as Radio-Frequency Ablation, in which this importance has been highlighted from early applications [7], to more recent studies [8], [9].

One option for monitoring temperature during laser ablation (LA) is to utilize Magnetic Resonance Imaging (MRI) in a technique known as MR thermometry [10]. This method is entirely non-invasive and offers high temperature sensitivity. However, it has notable limitations: the long acquisition times significantly reduce its ability to provide early warnings of potential hot spot formation that could lead to carbonization. Additionally, MR thermometry is highly sensitive to motion artifacts, which can further compromise its reliability in dynamic or real-time clinical settings.

Optical fiber-based sensors are excellent candidates for temperature measurement in the biomedical field due to their small form factor, immunity to electrical interference, and minimal self-heating when exposed to laser beams or other electromagnetic radiation sources, such as microwaves. Additionally, their reduced invasive impact makes them suitable for

This paper was produced by the IEEE Publication Technology Group. They are in Piscataway, NJ.

Manuscript received July 31, 2024; revised XXX YY, 2024.

All the authors are with the Department of Electronics and Telecommunications, Politecnico di Torino, Torino (Italy).  
(email: aurora.bellone@polito.it, massimo.olivero@polito.it, gianni.coppa@former.polito.it, alberto.vallan@polito.it, guido.perrone@polito.it)  
Digital Object Identifier:

use in surgical scenarios that require only light sedation. Furthermore, as all-dielectric structures, optical fiber sensors are fully compatible with MRI, enabling the integration of these two complementary techniques to maximize their benefits [11], such as compensate artifacts associated to MR imaging or mitigate the strain/temperature cross-sensitivity of optical fiber sensors [6].

The most widely used fiber optic temperature sensors are based on Fiber Bragg Gratings (FBGs) [12]. This well-established technology offers an exceptional balance of sensitivity, robustness, and manageable fabrication complexity, making it a reliable choice for various applications. As such, FBGs have extensively been used to measure the temperature during tumor ablation procedures [13]–[15]. An alternative is constituted by interferometric sensor relying on single mode - multi mode - single mode (SMS) structures, which are attractive for their higher sensitivity; however, SMS sensors cannot be used for the applications discussed in this paper because of their intrinsic long length that leads to strong limitations in terms of the achievable spatial resolution [16].

A drawback of FBG-based and of other fiber-based thermometers is the intrinsic cross-sensitivity between temperature and strain, which may introduce artifacts. In the experiments described in this paper strain-induced errors can be considered negligible because conducted on ex-vivo tissues and using power levels and exposure durations carefully set to avoid coagulation. In more realistic application scenarios, to mitigate the undesired effects of mechanical stress during temperature measurements, it is possible to protect the fiber with a capillary, compensate for strain effects, as done in [17], or use fiber sensors based on different technologies, such as those that rely on fluorescence decay time or on strain-insensitive Fabry-Perot cavities [18], [19].

In this work temperatures are measured with FBGs for their capability of being easily multiplexed along the same fiber to form arrays of FBG-thermometers. An FBG-thermometer array consists of a cascade of FBGs inscribed along the same fiber, usually using a femtosecond laser, but with slightly different reflection peak wavelength. Multiple FBG arrays can be simultaneously interrogated with a single instrument, hence they can be used to implement a quasi-distributed sensing system with millimeter-size spatial resolution [20]. FBG arrays have already been employed to reconstruct the temperature map during tumor thermal treatments [21], [22]; however, in some cases, as in the cited papers, FBG arrays are disposed to form grids around the applicator. This is an accurate approach to measure the obtained temperature distribution during lab experiments, but it is hardly applicable during actual surgeries, unless the minimally invasive requirement is released, with an increase in the patient discomfort. In previous papers we also demonstrated the possibility of combining laser delivery with temperature sensing capabilities using FBGs [23], [24].

To maintain a minimally invasive approach during laser ablation of internal organs implies that the temperature can be directly measured with optical fibers only by inserting a temperature sensor through the same needle used for the laser delivery fiber. In other words, the temperature can be measured only in the portion of the tissue close to the

laser delivery fiber; so, it is basically a one-dimensional measurement when a two- or three-dimensional map would be rather required. Therefore, the challenge becomes how to estimate the temperature distribution across the tumor volume from pinpoint temperature measurements taken along a line only. This represents a sort of ill-posed problem, but “good enough” estimates for the intended application can be obtained with prediction algorithms that extend the available measured data through simulations based on combined optical beam propagation and thermal models. In the simplest form, an estimation of the temperature map distribution across the entire area of interest can be obtained by solving a multi-physic model with the constrain that the predicted temperature along the delivery fiber has a good overlap with the measured temperature profile. Other more sophisticated methods can be used, but in any case the starting point is the knowledge of the biological tissue optical and thermal properties. However, these values are difficult to estimate since they cannot be taken from literature data or obtained from previous experiences given the variability typical of biological tissues, not only from individual to individual, but also within the organ itself. Therefore, they must be evaluated from some measurements that must be conducted directly on the target organ before the ablation procedure. In particular, we propose to evaluate such thermal parameters using the Heat Pulse Method (HPM), a transient technique based on the characterization of the radial transport of short-duration heat sources [25], [26]. This approach is widely applied to characterize soil (for example to determine the water content, besides for its thermal properties), but so far practically never used in biomedical applications. Clearly, soil differs significantly from biological tissue; moreover, HPM, at least in its classical implementation, assumes a homogeneous medium – an assumption that biological tissues typically do not satisfy due to their inherent heterogeneity. Nevertheless, these limitations can be addressed if, as detailed later, the goal is not to determine the exact value of the physical parameters, but rather to derive “equivalent” tissue thermal parameters. While these equivalent parameters may not have a direct numerical correspondence with the physical quantities, they can still be effectively used to accurately predict temperatures at locations where direct measurements are not feasible. The model can be considered an empirical approach that takes advantage of certain a-priori knowledge about the thermal behavior of laser-tissue interactions. It occupies a middle ground between a comprehensive thermal model, which precisely describes heat distribution, and a numerical or deep learning-based model, whose “black box” methodology neither utilizes a-priori information nor provides a physical interpretation of the results.

The goal of evaluating the temperature distribution map during a laser ablation procedure without worsening the invasive impact to continuously optimize the laser parameters is very ambitious. In another paper we have already analyzed some aspects related to the reconstruction of the temperature map from partial measurements through suitable hyperthermal treatment planning models based on the bio-heat equation [27]. However, this method has the weak point of requiring the knowledge of the physical thermal parameters, which are

difficult to estimate, as already discussed.

The approach proposed in this paper, which extends the work described in [17], is based on the experimental analysis of the tissue thermal behavior during the laser ablation procedure. In its basic steps the approach can be summarized as follows. First the laser is driven to deliver a rectangular heat pulse, whose effect is a temperature increase that depends on the tissue thermal parameters and on the distance between the laser delivery fiber tip and the point in which the temperature is measured. This temperature variation due to the laser pulse is measured close to the fiber tip using an FBG-based sensor. In the experiments described in this work the temperature is measured using a second optical fiber positioned parallel and close to the laser delivery fiber, so that the setup is similar to what described in [28], where a radio-frequency probe with two parallel needles is disclosed. However, as already mentioned, a configuration that combines in the same fiber the delivery and the sensing is possible [23], [24]. Then, the temperature evolution in response to the initial heat pulse – both during the heating and the cooling phases – is used to evaluate the tissue parameters by fitting the measured data in two locations to an analytical model. Finally, from these parameters, the temperature distribution at any arbitrary position can be obtained using the already mentioned analytical model.

The activity presented in this paper represents a first step towards the more general framework aimed at developing a tool that can predict the temporal evolution of the temperature map in the patient-specific tumor area as a function of the laser parameters (essentially, the power and the duration of irradiation). Patient-specific means that the tissue thermal and optical (not addressed in this paper) parameters must be evaluated for the specific tumor location in each patient. In this paper we propose to do it by recovering the thermal parameters from the response to an initial heat pulse. The preliminary validation of the proposed approach has been carried out in simplified case constituted by tests with ex-vivo samples. This is a foundational work and constitutes an essential step towards more comprehensive laboratory validations and, potentially, pre-clinical studies in the future.

The remaining of the paper is organized as follows. Sec. II solves analytically the problem of the temperature distribution due a rectangular heat pulse; then Sec. III describes the experimental setup. Sec. IV presents the obtained results, organized in two tests carried out on two different liver and with slightly different conditions to start addressing the problem of repeatability, in a test to analyze the impact of the uncertainty in the position of the temperature sensing fiber and in a test to evaluate the ability of the proposed approach to predict the temperature also close to the delivery fiber tip. Finally, Sec. V draws the conclusions.

## II. TEMPERATURE DISTRIBUTION IN THE PRESENCE OF A RECTANGULAR HEAT PULSE

The Heat Pulse Method (HPM) is a well-established technique for the determination of the thermal properties of a medium by fitting the experimentally obtained thermal impulse response – also called the thermal Green’s function – to its

analytical or numerical counterpart. Currently, this method is mainly employed to determine the physical parameters of soil, such as conductivity, heat capacity, and diffusivity [29]–[31]; in this paper we propose to extend its applicability to the biomedical field for determination of thermal parameters of tissue. As mentioned in the introduction, due to the approximations in our fitting model, the recovered thermal parameters should be interpreted as a set of values that, while individually they may not correspond to the expected physical values, can nonetheless be used collectively as “equivalent parameters” to accurately estimate the temperature at the desired locations.

Theoretically, the determination of the Green’s function would require an impulsive delta function source, both in time and in space, which is clearly unfeasible. However, close-form expressions can be also found for sources having Gaussian space distribution with spherical symmetry. This case is particularly relevant to our application, as the heat distribution can be approximately modeled in terms of Gaussian functions because the heat generated is proportional to the light intensity, and laser beams are often approximated as Gaussian beams. Additionally, the scattering and absorption phenomena lead to a rapid decay of the laser beam along its propagation direction, further reinforcing the Gaussian shape of the heat distribution.

As described in the heat pulse method [25] for the case of a constant power released over a time span  $t_{ON}$ , the temperature can be written in close-form as:

$$\begin{aligned}
 & \text{for } 0 \leq t \leq t_{ON} \\
 & T(r, t, \alpha, Q, t_s) = \frac{Q}{\alpha r} \left[ \operatorname{erfc} \left( \sqrt{\frac{r^2}{4\alpha(t+t_s)}} \right) + \right. \\
 & \qquad \qquad \qquad \left. - \operatorname{erfc} \left( \sqrt{\frac{r^2}{4\alpha t_s}} \right) \right] \\
 & \text{for } t \geq t_{ON} \\
 & T(r, t, \alpha, Q, t_s) = \frac{Q}{\alpha r} \left[ \operatorname{erfc} \left( \sqrt{\frac{r^2}{4\alpha(t+t_s)}} \right) + \right. \\
 & \qquad \qquad \qquad \left. - \operatorname{erfc} \left( \sqrt{\frac{r^2}{4\alpha(t+t_s-t_{ON})}} \right) \right] \tag{1}
 \end{aligned}$$

where  $\alpha$  is the thermal diffusivity,  $Q$  is related the quantity of heat delivered by the source,  $t_s$  is a “time-equivalent” of the heat source extension being the spatial width of the Gaussian source  $\sigma_s^2 = 2\alpha t_s$ ,  $r$  is the distance between the thermal source (the laser fiber tip in the considered case) and the point in which the temperature  $T$  is evaluated, as in Fig. 1-a. Note that  $Q$  and  $t_s$  take into account the source power and geometry. The thermal diffusivity is  $\alpha = k/(\rho C)$ , being  $k$  the tissue thermal conductivity,  $\rho$  the tissue density, and  $C$  the tissue heat capacity.

In the experimental setup, the laser is activated for a duration  $t_{ON}$  ranging from a fraction of a second to several seconds, long enough to induce a temperature transient with

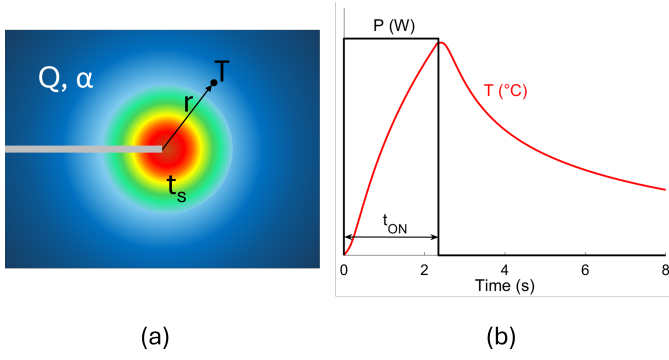


Fig. 1: Schematic of the Heat Pulse Method. (a): A spatially Gaussian heat pulse is generated at the laser delivery fiber tip. The parameters  $Q$  and  $t_s$  take into account the heat delivered by the source and the equivalent width of the source, respectively. (b): Example of the thermal response  $T$  at distance  $r$  from the source due to a heat pulse with duration  $t_{ON}$ .

a sufficiently high signal-to-noise ratio for recovering the tissue's thermal parameters. After the laser is turned off, the temperature returns to baseline (see Fig. 1-b), following a pattern that is primarily influenced by the distance from the source.

During an actual ablation procedure, Eq. 1 can be first employed to estimate the parameters  $Q$ ,  $\alpha$ , and  $t_s$  by fitting the equation to the temperature evolution recorded during a heat pulse test. Then, the same Eq. 1 can be used to predict the temperature in different positions. Clearly, the larger the number of fitting points, the more accurate will be the estimation of the parameters: for this reason, in the experiments the temperature was recorded during both the heating and cooling phases.

It is important to emphasize that the model represented by Eq. 1 does not fully capture the actual physical reality. For instance, it assumes a homogeneous tissue, whereas biological tissues are inherently heterogeneous. Consequently, the parameters derived from the fitting procedure should be regarded as “equivalent” thermal parameters rather than quantities with precise physical value. As will be demonstrated in the experimental section, these equivalent parameters can nonetheless be effectively used to predict temperature values at locations where direct measurements are not feasible.

#### A. Heat pulse method for non-Gaussian sources

The solution of the heat diffusion problem in Eq. 1 is only valid when the heat source has isotropic Gaussian distribution and the irradiated tissue is homogeneous. These hypotheses are hardly fulfilled in practical laser ablation treatments because of the non uniformity both due to the tissue and to the emission around the delivery fiber, which predominantly concentrated in front of the tip. Nevertheless, the optical power is mainly dissipated in a hot spot located at the fiber output, which is small with respect to the dimensions of the heated tissue. This is because biological tissues, like liver, have typically large scattering and absorption coefficients. Therefore, in this

scenario the asymmetry of the hot spot become less relevant, albeit it is still responsible for large errors in some applications. A solution to this problem could be to represent the actual optical source as the sum of a large number of ideal Gaussian sources; however, this approach is not feasible in practice because it would require the determination of quite a large number of parameters and this means long processing times. Having experimentally verified that, for the cases considered in this paper, decomposing the heat source into three or more Gaussian functions does not result in significant improvements in accuracy (see also Sect. IV), we opted for a decomposition into two Gaussian sources. The parameters of these two sources are obtained through the aforementioned fitting procedure. A thermal model that incorporates a heat source made by the superposition of two Gaussian contributions, is thus given by 2:

$$T^{2G}(r, t) = T(r, t, \alpha, Q_1, t_{s1}, ) + T(r, t, \alpha, Q_2, t_{s2}) \quad (2)$$

where  $Q_1$ ,  $t_{s1}$ ,  $Q_2$ ,  $t_{s2}$  are the parameters describing the two Gaussian distributions, respectively. The advantage of using this approach in real applications will be shown in the Experimental Results section.

Then, to make the fitting procedure more robust and less sensitive to the tissue non-uniformity, temperature measurements are taken at two points rather than at a single point, as done in [17]). Specifically, temperatures  $T_{m1}$  and  $T_{m2}$  are measured at two known distances  $r_1$  and  $r_2$  from the fiber tip. The parameters  $\alpha$ ,  $Q_1$ ,  $t_{s1}$ ,  $Q_2$  and  $t_{s2}$  are estimated by minimizing the square error  $SE$  in Eq. 3 between the measured temperatures  $T_{m1}$ ,  $T_{m2}$  and their respective predictions  $T^{2G}(t, r_i)$  evaluated at their measurement positions, as in Eq. 4:

$$SE = \sum_t [T^{2G}(t, r_1) - T_{m1}(t)]^2 + \sum_t [T^{2G}(t, r_2) - T_{m2}(t)]^2 \quad (3)$$

$$\min_{\alpha, C_1, t_{s1}, C_2, t_{s2}} (SE) \quad (4)$$

Overall, these solutions represent a significant improvement with respect to the previous implementation of the HPM presented in [17].

### III. SETUP DESCRIPTION

The experimental activity was conducted on ex-vivo bovine liver tissue, irradiated with a laser light at 975 nm from a high-power semiconductor laser coupled into a 600  $\mu\text{m}$  core – 1 mm total diameter fiber. The tip of the fiber was cleaved and encapsulated in a glass capillary with internal diameter of 1 mm and outer diameter of 1.5 mm. The probe is placed between two slices of ex-vivo bovine liver, each one 2 cm thick.

The optical source was reconstructed as the sum of two Gaussian curves, as described in Sec. II-A, and the fitting is performed using the all set of temperatures measured at two different points.

The sensing fiber used for the temperature measurement is a bare glass fiber that embeds an array of 20 FBGs with 1 mm length each and 1 mm spacing between each FBG; hence the spatial resolution in terms of the distance between two consecutive measurement points is 2 mm. The FBGs were inscribed into the fiber core using a femtosecond laser with the Point-by-Point technique. The array was then characterized as described in [17]. One should note that the validation of the thermal model does not require knowledge of the absolute temperature value but only the measurement of the temperature change from steady-state conditions. To this aim only the sensor sensitivity is of interest. The sensors were read using a four-channel Luna's HYPERION si155 interrogator, which implements a tunable laser FBG interrogation scheme. Differently from the sensors employed for the preliminary tests described in [17], the sensing fibers used in the tests described in the following are not encapsulated in capillaries to reduce the effects of possible mechanical stresses that could occur during coagulation [32]. This choice, however, significantly lowers the perturbation induced by these additional fibers to the thermal model and the overall invasive impact. Anyway, special care was taken in positioning the sensor and preventing any mechanical stress during the tests. Future improvements could include techniques to discriminate between temperature and strain, such as those based on FBGs inscribed in multicore fibers [33] or the usage of different fiber sensors insensitive to strain. The results presented in the following only report the temperature change  $\Delta T$  with respect to the initial temperature. For this purpose, the calibration procedure is only employed to estimate FBG sensitivity coefficients.

The sensor array is positioned as shown in Fig. 2. The sensing point #10 and the following #11 are located close to the fiber tip and thus to the heat source. They are employed as measurement points to feed the fitting algorithm. The sensing points from #12 to #20 are employed for comparison purposes to assess the ability of the proposed procedure to predict the temperature away from the measurement points. Sensing points from #1 to #9 are employed to highlight possible distortion in the temperature profile introduced by the delivery fiber, but their outputs are not shown in this paper. This setup is specific to the characterization tests conducted for validation; in possible clinical applications a single applicator capable of measuring in just two points obtained by a sensing fiber coincident with the delivery fiber or close to it will be necessary.

#### IV. EXPERIMENTAL RESULTS

Several tests have been carried out on different biological tissues, placing the sensing fiber at different distances  $d$  from the delivery fiber and varying the laser power and the exposure time. The sensitivity of the results with the distance  $d$  has been also analyzed.

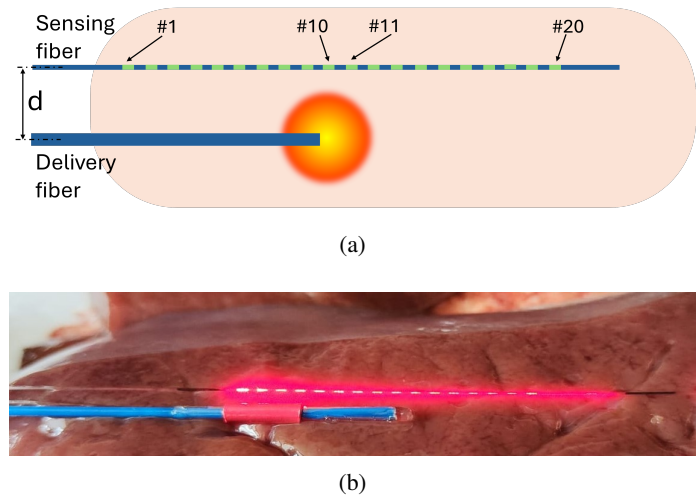


Fig. 2: Experimental setup for the irradiation and sensing of ex-vivo bovine liver tissue. (a): sketch. (b): picture. The thick blue probe is the delivery fiber, while the transparent bare fiber is the sensing fiber that contains 20 equally spaced FBGs. A red light was launched into the sensing fiber to evidence the position of the FBGs.

##### A. Test on liver sample #1

In the first test the distance between the sensing and delivery fibers was 3.5 mm and the biological tissue was irradiated for 4 s with a power of 3.4 W. The temperature along the sensing fiber was acquired for a total of 14 s. The measurements obtained from the FBG array are reported in Fig. 3, in which FBG#10 registered the highest temperature, as expected being the closer to the fiber tip. A more careful examination of these curves shows that temperatures increase even after the laser was turned off. This seemingly counter-intuitive rise in temperature immediately after the laser is switched off can be attributed to the relatively slow propagation of heat compared to the rapid switching-off time of the laser. Indeed, the sensing points are positioned along the fiber at increasing distances from the delivery fiber, starting with FBG#10, which is 3.5 mm away, so that each sensor detects a temperature increase only after a certain delay. In other words, it takes some time for each sensor to “sense” changes in the laser’s status.

Fig. 4 shows (a) the results of the fitting algorithm for the first tests and (b) the residual of the fitting, that is, the difference between the measured temperature and the temperature obtained fitting the measured one. To provide a statistical evaluation of the fitting capability of the model, the root mean square error (RMSE) was evaluated from the data of Fig. 4b, yielding  $0.039^\circ\text{C}$  and  $0.064^\circ\text{C}$  for sensor #10 and sensor #11, respectively.

As pointed out in Sect. I, the thermal model has not been devised for the measurements of the thermal parameters but for the temperature prediction close to the measurement points. Actually, in this test, the recovered equivalent thermal diffusivity in Eq. 1 turned out to be  $\alpha = 0.17 \text{ mm}^2/\text{s}$ , a value close

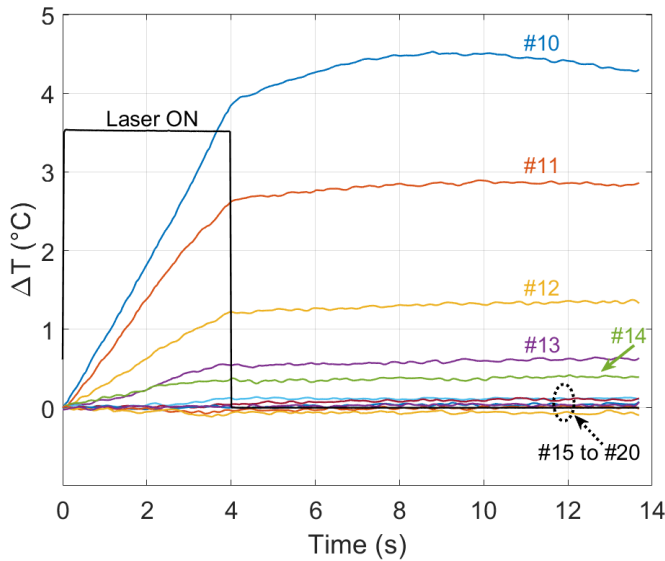


Fig. 3: Temperature registered by the sensing fiber during the first test. The figure reports the readings from FBG#10 to FBG#20, while the black line indicates the duration of the laser irradiation.

but significantly different from the result  $\alpha = 0.14 \text{ mm}^2/\text{s}$  obtained in [34] testing a similar tissue.

Once the thermal parameters have been obtained from the fitting procedure, they can be used to estimate the temperature at different distances and positions. For example, Fig. 5 compares the temperature predicted along the sensing fiber (blue line) with the temperature measured using the FBGs (red circles, corresponding to the sensing points from #10 to #20) for different times. The bold circles identify the sensing point #10 and #11 in which the temperatures employed for the fitting were recorded. The agreement between predictions and measurements is very good: the almost perfect overlapping at the two fitting points was expected given the excellent agreement of the curves in Fig. 4, while at the other positions the maximum difference is of about  $0.25 \text{ }^\circ\text{C}$ .

The results of this test also suggest that a smart applicator able to simultaneously deliver the laser beam and accurately predict the temperature in the region in front of it can be assembled by complementing the delivery fiber with a short sensing fiber that protrudes just for about 2 mm (i.e., up to FBG #11) to have at least two fitting points.

To highlight the improvement of modeling the heat source using two Gaussian distributions, the data from the first experiment were also processed using a thermal model based on a single Gaussian source. The fitting error increases to  $0.5 \text{ }^\circ\text{C}$  and the prediction capability becomes less accurate with a maximum error of about  $0.4 \text{ }^\circ\text{C}$  (Fig. 6). Using more than two Gaussian distributions does not provide significant advantages in terms of accuracy, while the processing time strongly increases: for example, in the case of three Gaussian distributions, it becomes about five times larger than in the case of two sources.

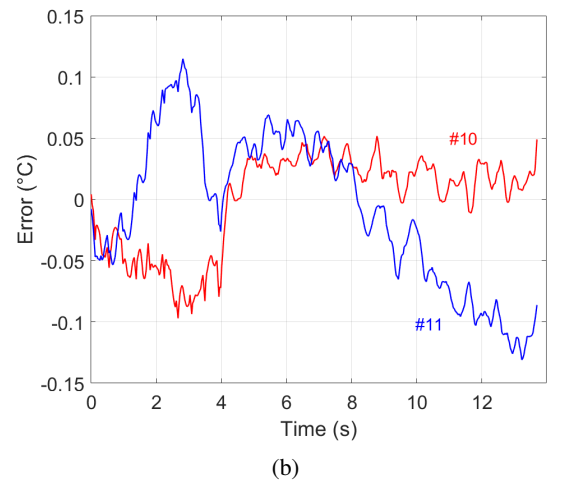
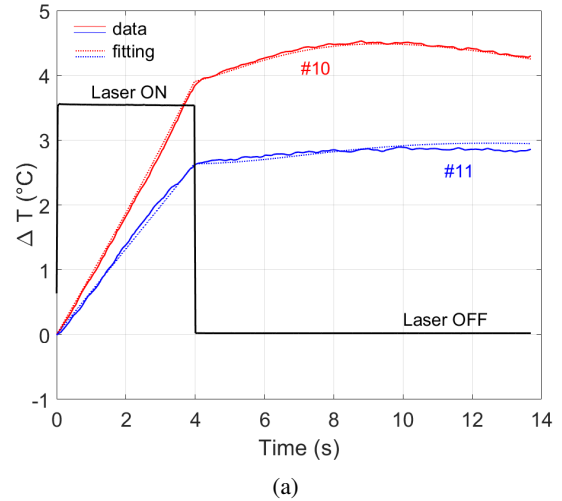


Fig. 4: Results of the fitting algorithm for the first test. (a): the measured temperatures at the positions of the FBGs #10 and #11 and the corresponding curves fitting the experimental data according to the model of Eqn. 1. (b): residual fitting errors.

### B. Tests on liver sample #2

A second test was conducted using the same delivery fiber but a different liver sample. In this case, the distance between the two fibers was  $d = 4 \text{ mm}$  and the laser was activated for 8 s. Compared to the first test, the laser energy was approximately 50% greater, while the sensing fiber was positioned slightly farther away. The temperatures acquired at positions #10 and #11 (Fig. 7a) show a smaller and delayed temperature peak. This behavior is difficult to predict due to the inherent variability in liver parameters, which are challenging to anticipate. For example, in ex-vivo cases liver characteristics depend on the water content, which in turn depends on the freshness of the sample, while in in-vivo they are influenced by proximity to major blood vessels. These factors highlight the importance of continuous temperature monitoring during laser ablation procedures.

Quantitatively, in this case, the root mean square error

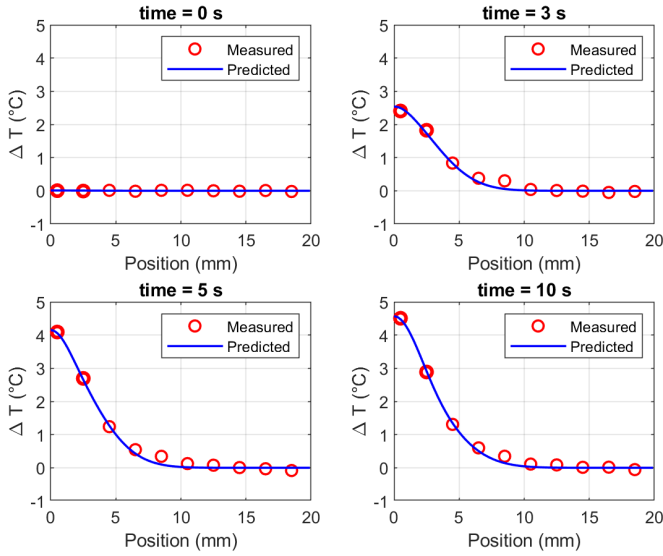


Fig. 5: Comparison between measured and predicted temperatures at four time instants (0, 3, 5 and 10 s) in the conditions of the first test. The red circles are the temperatures measured from the corresponding FBGs; the blue solid line is the temperature predicted by the thermal model based on two Gaussian sources.

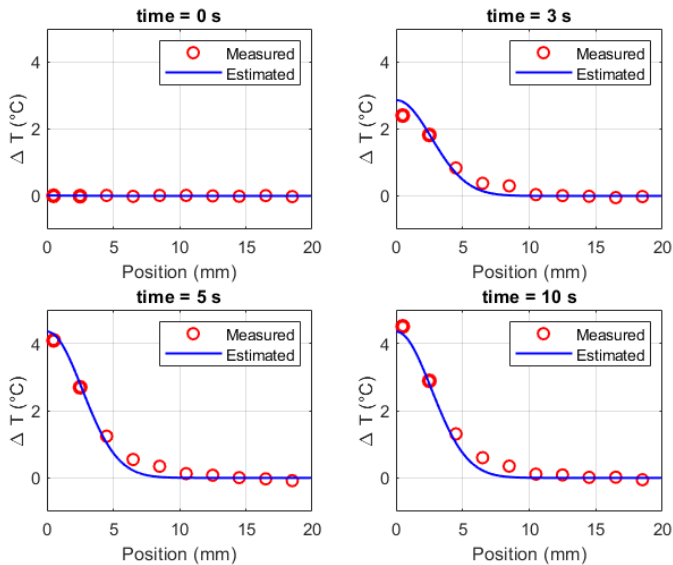


Fig. 6: Comparison between measured and predicted temperatures at four time instants (0, 3, 5 and 10 s) in the conditions of the first test. The fitting model is based on a single Gaussian source.

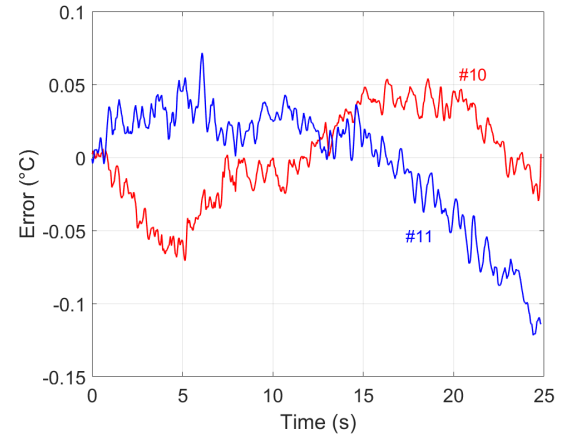
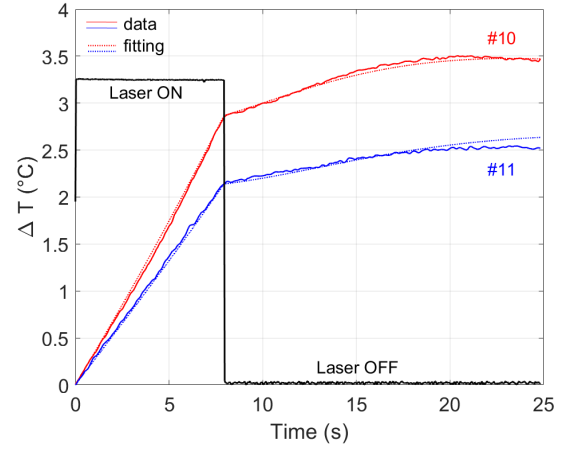


Fig. 7: Results of the fitting algorithm for the second test. (a): the measured temperatures at the positions of the FBGs #10 and #11 and the corresponding curves fitting the experimental data according to the model of 1. (b): residual fitting errors.

RMSE, evaluated from the data of Fig. 7b, were  $0.033^{\circ}\text{C}$  and  $0.042^{\circ}\text{C}$  for sensor #10 and sensor #11, respectively. These values are of the same order of magnitude of those calculated for the first test, yet slightly lower. The equivalent thermal diffusivity recovered in experiment (i.e., with this setup and liver sample) is  $\alpha = 0.079\text{mm}^2/\text{s}$ , a value that presents a significant difference with respect to that reported in [34]. Nevertheless, the results in Fig. 8 show again a good agreement between predicted and measured temperature values.

*C. Sensitivity to the distance between the delivery and sensing fibers*

The proposed model is based on the accurate knowledge of the sensing fiber position. However, the distance  $d$  was measured with a ruler and it is thus affected by an uncertainty that reflects on the temperatures predicted by the model. The conventional method for the uncertainty propagation cannot

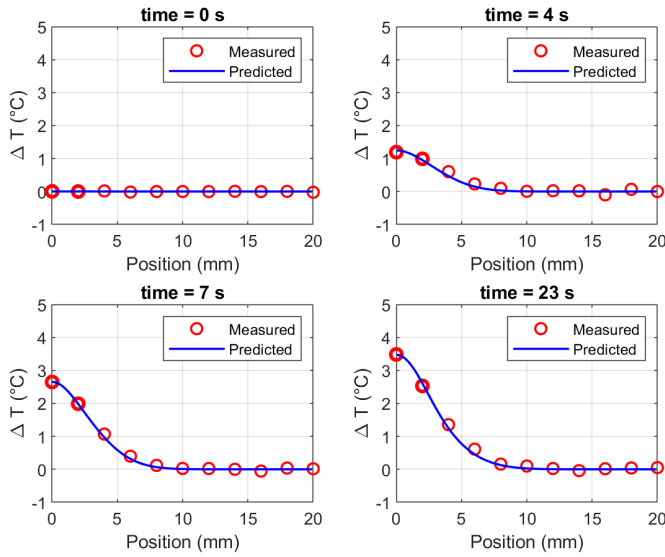


Fig. 8: Comparison between measured and predicted temperatures at four time instants (0, 4, 7 and 23 s) in the conditions of the second test. The red circles are the measured temperatures, while the blue solid line is the temperature predicted by the thermal model.

be here employed since the results depends on a fitting algorithm and it is not possible to write a function that describes the measurement model. Anyway, the uncertainty effects can be highlighted simply by running the fitting and the reconstruction algorithm while modifying the nominal value of the distance  $d$ . Considering in particular the second test conditions, errors from  $-0.5$  mm to  $1$  mm were introduced in the nominal value of  $d$  (i.e., around  $4$  mm). Fig. 9 shows the predicted temperature distribution at the end of the test. The maximum deviation is of about  $0.1$  °C, a value that can be considered comparable with the fitting errors. The low sensitivity with the sensing fiber distance is due to the fitting algorithm that takes advantage of two sensing points located at a relative distance that is known with a very good accuracy because the extremely high accuracy of the FBG inscription process using a femtosecond laser.

#### D. Evaluation of the prediction capabilities close to the delivery fiber tip

The results presented so far confirm that the proposed method can effectively indirectly measure the temperature in locations within the treated area, but having an offset with respect to the delivery fiber. However, during an actual ablation procedure, the primary focus is on the temperature of area in front of the delivery fiber. To evaluate the method's ability to predict temperature values also in this region, the experimental setup was modified by adding a second sensing fiber along the axis of the delivery fiber, as shown in Fig. 10. The goal of this additional test is to complement the assessment of the performance of the thermal model and demonstrate that it can be used to estimate the temperature at any point within the treatment zone. Thus, it should be noted that the second sensing fiber is added for validation purposes only and it

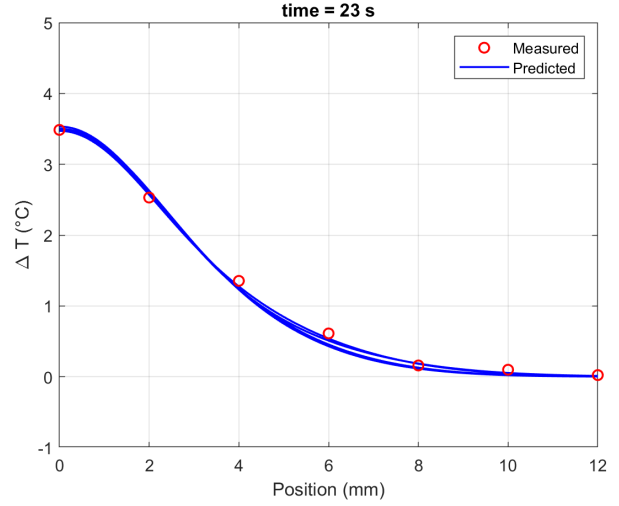


Fig. 9: Temperature predicted along the sensing fiber considering distance  $d$  affected by uncertainty. The bundle of blue lines were obtained by processing the measurements in Fig. 7a when the value of  $d$  varies in the range of  $3.5$  mm to  $5$  mm (second test, nominal value  $4$  mm).

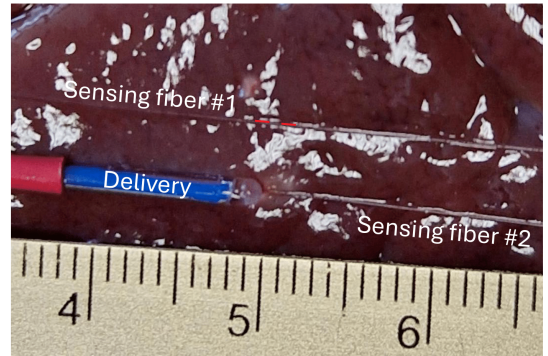


Fig. 10: Setup with two sensing fibers. Red lines on sensing fiber #1 are the points where temperatures are measured.

is not necessary for the implementation of the measurement approach. The second sensing fiber is identical to the first one and was positioned with its first FBG as close as possible to the delivery tip. For mechanical reasons this minimum distance was about  $2.5$  mm; therefore, the hottest point, which is expected to be directly on the fiber tip, could not be measured with this setup.

Fig. 11 shows the temperature reconstructed along the second sensing fiber using the thermal parameters obtained by processing the temperature measurements from the FBGs #10 and #11 of the first sensing fiber as described in the previous sections and reported in Fig. 8. The comparison between reconstructed and measured temperature is only possible from the first available sensor, which as already mentioned is at about  $2.5$  mm from the delivery fiber end-facet. The temperatures along the second sensing fiber are much larger than those recorded by the first fiber because the distance from heat source is smaller. Anyway, also in this case the difference between predicted and measured values is low, below  $2$  °C, values that are well within the acceptable ranges for laser

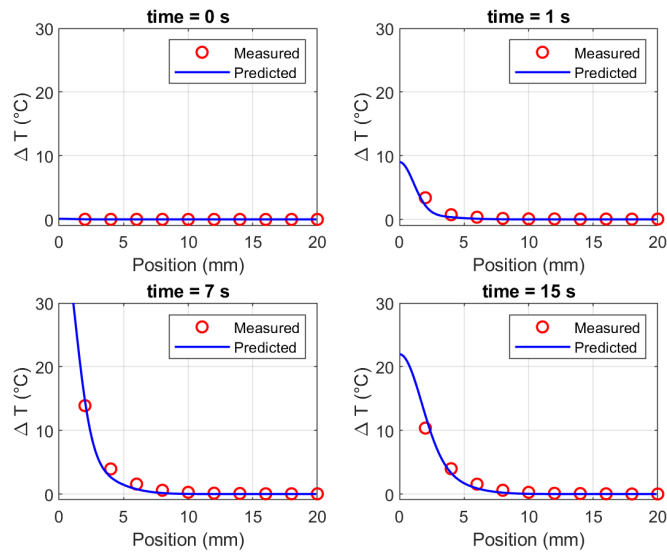


Fig. 11: Temperature predicted along the delivery fiber in the conditions of the second test.

ablation procedure.

## V. CONCLUSION

Monitoring of the temperature is fundamental for the optimal outcome of thermal treatments of tumors, especially in the case of high-temperature treatments, such as laser ablation. Considering internal organs, this requires contact sensors and to minimize the patient discomfort they should have the minimal possible invasive impact. However, this essential requirement from the patient viewpoint contrasts with the necessity of the surgeon to have the temperature map across the entire tumor area.

The paper has presented a method to predict the temperature distribution around the laser delivery fiber in a minimally invasive way because it relies on the temperature measured in just two points in close proximity of the laser delivery fiber.

The proposed algorithm uses the thermal Green's function, with patient-specific tissue thermal parameters obtained through a fitting procedure based on temperature evolution measurements at two known positions. This approach makes the fitting more robust and less sensitive to the position of the sensing points and to the tissue non-uniformity, which represents a typical scenario during a real ablation.

The approach has been validated in post-processing through a series of tests carried out using different ex-vivo bovine liver samples. The results demonstrated a very good agreement between the predicted temperatures and the validation measurements, confirming the feasibility of predicting the temperature distribution across the entire ablated area with a level of accuracy suitable for this application. These findings demonstrate the potential of the method for practical implementation in laser ablation procedures.

However, while the ex-vivo results are promising, additional testing is essential to fully evaluate the robustness and versatility of the approach. A much larger dataset is needed to investigate its performance under varying measurement

conditions, going beyond bovine liver to assess the method's applicability to other clinical contexts where laser ablation is employed, such as human tissues with varying structures and properties. Testing under in-vivo conditions will also be necessary to address the challenges posed by motion, blood flow, and dynamic thermal effects, which are absent in ex-vivo scenarios but critical in real-world applications. By addressing these additional considerations, the method can be refined and its reliability firmly established for a broader range of clinical and practical applications.

## REFERENCES

- [1] C. Brace, "Thermal tumor ablation in clinical use," *IEEE Pulse*, pp. 28–38, 2011.
- [2] C. J. Diederich, "Thermal ablation and high-temperature thermal therapy: Overview of technology and clinical implementation," *Int. J. of Hyperthermia*, vol. 21, pp. 745–753, 2005.
- [3] F. Barbero, S. Gul, G. Perrone, and I. Fenoglio, "Photoresponsive inorganic nanomaterials in oncology," *Technology in Cancer Research & Treatment*, vol. 22, 2023.
- [4] P. Saccomandi, G. Quero, R. Gassino, A. Lapergola, L. Guerriero, M. Diana, A. Vallan, G. Perrone, E. Schena, G. Costamagna, J. Marescaux, and F. M. D. Matteo, "Laser ablation of the biliary tree: in vivo proof of concept as potential treatment of unresectable cholangiocarcinoma," *Int. J. of Hyperthermia*, vol. 34, pp. 1372–1380, 2018.
- [5] M. Ahmed, C. L. Brace, F. T. Lee, and S. N. Goldberg, "Principles of and advances in percutaneous ablation," *Radiology*, vol. 258, pp. 351–369, 2011.
- [6] M. D. Landro, J. Ianniello, M. Yon, A. Wolf, B. Quesson, E. Schena, and P. Saccomandi, "Fiber bragg grating sensors for performance evaluation of fast magnetic resonance thermometry on synthetic phantom," *Sensors*, vol. 20, no. 22, 2020.
- [7] J. Dinerman, R. Berger, and H. Calkins, "Temperature monitoring during radiofrequency ablation," *J. Cardiovasc Electrophysiol.*, vol. 7, pp. 163–173, 1996.
- [8] P. Saccomandi, G. Frauenfelder, M. C. C. Massaroni, A. Polimadei, F. Taffoni, F. D. Matteo, G. Costamagna, F. Giurazza, and E. Schena, "Temperature monitoring during radiofrequency ablation of liver: in vivo trials," in *Annu Int Conf IEEE Eng Med Biol Soc.*, 2016.
- [9] U. Longo, F. D. Tommasi, G. Salvatore, A. Lalli, D. L. Presti, C. Massaroni, and E. Schena, "Intra-articular temperature monitoring during radiofrequency ablation in ex-vivo bovine hip joints via fiber bragg grating sensors," *BMC Musculoskelet Disord.*, vol. 24, p. 766, 2023.
- [10] V. Rieke and K. B. Pauly, "Mr thermometry," *J Magn Reson Imaging*, vol. 27, 2008.
- [11] B. Patel and A. H. Kim, "Laser interstitial thermal therapy," *Mo Med*, vol. 117, pp. 50–55, Jan-Feb 2020.
- [12] W. Chen, R. Gassino, Y. Liu, A. Carullo, G. Perrone, A. Vallan, and D. Tosi, "Performance assessment of fbg temperature sensors for laser ablation of tumors," in *Proc. IEEE International Symposium on Medical Measurements and Applications (MeMeA)*, 2015.
- [13] E. Schena, D. Tosi, P. Saccomandi, E. Lewis, and T. Kim, "Fiber optic sensors for temperature monitoring during thermal treatments: an overview," *Sensors*, vol. 16, p. 1144, 2016.
- [14] G. Palumbo, A. Iadicicco, S. Campopiano, D. Tosi, E. Schena, C. Massaroni, N. Carlomagno, V. Tammara, P. Verze, and J. Ippolito, "Measurements of temperature during thermal ablation treatments on ex vivo liver tissue using fiber bragg grating sensors," in *2017 IEEE International Instrumentation and Measurement Technology Conference (I2MTC)*, pp. 1–6, 2017.
- [15] S. Korganbayev, A. Orrico, L. Bianchi, M. D. Landro, A. Wolf, A. Dostovalov, and P. Saccomandi, "Closed-loop temperature control based on fiber bragg grating sensors for laser ablation of hepatic tissue," *Sensors*, vol. 20, p. 6496, 2020.
- [16] M. Olivero, A. Vallan, R. Orta, and G. Perrone, "Single-mode-multimode-single-mode optical fiber sensing structure with quasi-two-mode fibers," *IEEE Trans. Instr. Meas.*, vol. 67, pp. 1223–1229, 2018.
- [17] A. Bellone, E. Ullo, M. Olivero, G. Coppa, A. Vallan, and G. Perrone, "Preliminary analysis of the estimation of tissue thermal parameters for tumor laser ablation with minimally invasive techniques," in *2024 IEEE International Instrumentation and Measurement Technology Conference (I2MTC)*, 2024.

- [18] K. Yang, Y. Shen, K. He, T. Zhang, R. Xu, S. Zhao, L. Chen, and S. Xu, "An optical fiber temperature sensor based on fluorescence intensity ratio used for real-time monitoring of chemical reactions," *Ceramics International*, vol. 47, 2021.
- [19] Q. Liu, D. Wang, C. Wang, H. Gao, and F. Cheng, "Ultrasensitive temperature sensor based on optical fiber fabry-pérot interferometer with vernier effect," *Optics Communications*, vol. 541, 2023.
- [20] A. Beccaria, A. Bellone, A. Mirigaldi, V. Serafini, M. Olivero, A. Vallan, and G. Perrone, "Temperature monitoring of tumor hyperthermal treatments with optical fibers: comparison of distributed and quasi-distributed techniques," *Optical Fiber Technology*, vol. 60, p. 102340, 2020.
- [21] G. Palumbo, E. D. Vita, E. Schena, C. Massaroni, P. Verze, N. Carlo-magno, V. Tammaro, R. L. Rocca, J. Ippolito, D. Tosi, P. Saccomandi, M. A. Caponero, A. Iadicicco, and S. Campopiano, "Multidimensional thermal mapping during radiofrequency ablation treatments with minimally invasive fiber optic sensors," *Biomed. Opt. Express*, vol. 9, pp. 5891–5902, 2018.
- [22] F. Santucci, M. Nobili, F. D. Tommasi, D. L. Presti, C. Massaroni, E. Schena, and G. Oliva, "Optimizing sensor placement for temperature mapping during ablation procedures," *Sensors*, vol. 24, p. 623, 2024.
- [23] Y. Liu, R. Gassino, A. Braglia, A. Vallan, and G. Perrone, "Fibre probe for tumour laser thermotherapy with integrated temperature measuring capabilities," *Electronics Letters*, vol. 52, pp. 798–800, 2016.
- [24] R. Gassino, Y. Liu, M. Konstantaki, A. Vallan, S. Pissadakis, and G. Perrone, "A fiber optic probe for tumor laser ablation with integrated temperature measurement capability," *Journal of Lightwave Technology*, vol. 35, pp. 3447–3454, 2017.
- [25] H. He, M. F. Dyck, R. Horton, T. Ren, K. L. Bristow, J. Lv, and B. Si, "Development and application of the heat pulse method for soil physical measurements," *Reviews of Geophysics*, vol. 56, pp. 567–620, 2018.
- [26] M. B. de Moraes França, F. J. O. Moraes, P. Carvalhaes-Dias, L. C. Duarte, and J. A. S. Dias, "A multiprobe heat pulse sensor for soil moisture measurement based on pcb technology," *IEEE Trans. Instr. Meas.*, vol. 68, pp. 606–613, 2019.
- [27] R. Gassino, J. Pogliano, G. Perrone, and A. Vallan, "Temperature distribution mapping using an fbg-equipped probe for solid tumor laser ablation," in *IEEE International Symposium on Medical Measurements and Applications (MeMeA)*, pp. 1–6, 2018.
- [28] R. Geoghegan, A. Santamaria, A. Priester, L. Zhang, H. Wu, W. Grundfest, L. Marks, and S. Natarajan, "A tissue-mimicking prostate phantom for 980 nm laser interstitial thermal therapy," *Int. J. of Hyperthermia*, vol. 36, pp. 992–1001, 2019.
- [29] M. E. O. Firat, "Experimental study and modelling of the thermal conductivity of frozen sandy soil at different water contents," *Measurement*, vol. 181, p. 109586, 2021.
- [30] Y. Kojima, J. L. Heitman, K. Noborio, T. Ren, and R. Horton, "Sensitivity analysis of temperature changes for determining thermal properties of partially frozen soil with a dual probe heat pulse sensor," *Cold Regions Science and Technology*, vol. 151, pp. 188–195, 2018.
- [31] K. S. Patle, V. Panchal, R. Saini, Y. Agrawal, and V. S. Palaparthi, "Temperature compensated and soil density calibrated soil moisture profiling sensor with multi-sensing point for in-situ agriculture application," *Measurement*, vol. 201, p. 111703, 2022.
- [32] R. Gassino, G. Perrone, and A. Vallan, "Temperature monitoring with fiber bragg grating sensors in nonuniform conditions," *IEEE Trans. Instr. Meas.*, vol. 69, pp. 1336–1343, 2020.
- [33] L. Htein, D. S. Gunawardena, C. Y. Leong, and H. Y. Tam, "Bragg gratings in two-core rectangular fiber for discrimination of curvature, strain, and temperature measurements," *IEEE Trans. Instr. Meas.*, vol. 70, pp. 1–7, 2021.
- [34] S. R. Guntur, K. I. Lee, D.-G. Paeng, A. J. Coleman, and M. J. Choi, "Temperature-dependent thermal properties of ex-vivo liver undergoing thermal ablation," *Ultrasound Med. Biol.*, vol. 1771-84, 2013.